



## Preparation and characterization of photocatalytic TiO<sub>2</sub>/glymo nanocomposite films

Esin AKARSU<sup>1,\*</sup>, H. Erdem ÇAMURLU<sup>2</sup><sup>1</sup>Department of Chemistry, Faculty of Science, Akdeniz University, Antalya, Turkey<sup>2</sup>Department of Mechanical Engineering, Faculty of Engineering, Akdeniz University, Antalya, Turkey

Received: 12.02.2018

Accepted/Published Online: 07.08.2018

Final Version: 11.10.2018

**Abstract:** The reflux method was utilized for the synthesis of 5% Sn-doped TiO<sub>2</sub> nanopowder. Surfaces of the TiO<sub>2</sub> particles were modified with 3-glycidoxypropyltrimethoxysilane (glymo) and glass surfaces were coated with this solution by a spin-coating process. Molar ratios of TiO<sub>2</sub>:glymo were 0.25, 0.5, 2.5, and 7.5 in the films. Nanocomposite films were cured at 130 °C. Adhesions of the obtained films were classified as 5B and pencil hardness increased with the increase in the ratio of the TiO<sub>2</sub> in the films. Film thickness decreased from 5 μm to 0.3 μm when TiO<sub>2</sub>:glymo was increased from 0.25 to 7.5. The obtained films had sufficient mechanical integrity, and they were photocatalytically active and could degrade rhodamine B. The sample having a TiO<sub>2</sub>:glymo ratio of 7.5 presented the highest photoactivity. Low-temperature curing brings the advantage of utilization of the films on polymer substrates and also there is no need for a barrier layer between the coating and the substrate.

**Key words:** Photocatalytic film, glymo, TiO<sub>2</sub>, hybrid coating, photocatalysis

### 1. Introduction

To prevent environmental pollution, it is required to eliminate organic-based pollutants in aqueous solutions and the atmosphere before they are discharged into the environment, for which heterogeneous photocatalysts are attracting increasing attention. Upon exposure to a light source, pairs of electrons and holes form in semiconductor photocatalysts. These pairs produce oxygen and hydroxyl radicals, which are powerful to degrade organic-based substances by oxidation and reduction. Besides many semiconductors such as WO<sub>3</sub>, SnO<sub>2</sub>, ZrO<sub>2</sub>, and ZnO, TiO<sub>2</sub> has become popular due to its superior properties such as being chemically stable and nontoxic.<sup>1–3</sup> The anatase crystalline form of TiO<sub>2</sub> is widely used since charge carriers excited in the deeper bulk of anatase are more efficiently transported to the surface than in rutile.

A major drawback of TiO<sub>2</sub> for photocatalytic applications is its wide band gap (E<sub>g</sub> = 3.2 eV), which limits its use solely to UV light. Therefore, TiO<sub>2</sub> photocatalysts cannot utilize most of the solar irradiation (~95%). The doping of the TiO<sub>2</sub> crystalline structure with metal ions has been extensively studied to shift its band gap into the visible region. Another outcome of ion doping, when used in right amounts, was proposed to be the suppression of the hole–electron recombination.<sup>4,5</sup> The effect of various metal ions such as Al<sup>3+</sup>, V<sup>5+</sup>, Cr<sup>3+</sup>, Mn<sup>2+</sup>, Fe<sup>3+</sup>, Zn<sup>2+</sup>, Sn<sup>4+</sup>, and Ce<sup>4+</sup> on the photocatalytic activity of TiO<sub>2</sub> has been studied in literature.<sup>6–14</sup> It was reported that a proper amount of the dopant, which depends on its type, enhances the photoactivity of TiO<sub>2</sub> under UV and visible irradiation.<sup>7,11,12,14–16</sup> Sn was doped in TiO<sub>2</sub> films and powders

\*Correspondence: esinburunkaya@gmail.com

and its effects were investigated. As a result, 5% Sn was reported to enhance the photoreactivity of  $\text{TiO}_2$ . One benefit of dopants was suggested as reducing the particle size and increasing the surface area, thus providing higher adsorption, which constitutes the first step of the photocatalytic process. Another benefit was suggested as creating new electronic states in the band gap of  $\text{TiO}_2$ , and separation of the charge carriers.<sup>10,11,17</sup>

Photocatalysts are applied in the form of both powder and coating. In the case of the utilization of powdered photocatalysts, they have to be removed from slurry in the reaction chamber by filtering at the end of photodegradation process. The fact that the filtration of nanoparticles is difficult to accomplish makes processes involving use of powdered  $\text{TiO}_2$  nanoparticles not feasible for continuous flow systems.<sup>4</sup> Use of photocatalysts as thin films has eliminated these difficulties. Even though the photocatalytic efficiency of powders is superior to that of films due to the much larger surface area of powders, films are commonly used because of their easier application.<sup>1,18,19</sup>

$\text{TiO}_2$  films were obtained by utilizing various methods such as supersonic cluster beam deposition,<sup>20</sup> magnetron sputtering,<sup>21</sup> hydrothermal,<sup>22</sup> and sol-gel syntheses.<sup>23–26</sup>

In most of the methods,  $\text{TiO}_2$  films are obtained from polymeric sols or colloidal sols and a calcination step is necessary for densification and to obtain the anatase crystal structure of the  $\text{TiO}_2$  film. Calcination is conducted at about 500 °C since the temperature of crystallization for anatase is lower than that for rutile.<sup>18,19,25,26</sup> During calcinations, two undesired phenomena take place. One is the growth of  $\text{TiO}_2$  particles and the other is  $\text{Na}^+$  ion diffusion from soda-lime glass substrate into the  $\text{TiO}_2$  layer.<sup>9,25,26</sup> The presence of Na is undesired in  $\text{TiO}_2$  and it deteriorates the properties of  $\text{TiO}_2$ .<sup>26</sup> A barrier layer is required in order to prevent the contact of the  $\text{TiO}_2$  layer with the glass substrate.<sup>26</sup> On the other hand, in hydrothermal and reflux methods, the crystalline anatase phase of  $\text{TiO}_2$  can be obtained when the conditions are right. Therefore, in these methods, the calcination step can be avoided. As a result, grain growth and Na contamination of the  $\text{TiO}_2$  film can be prevented.

In a previous paper,<sup>17</sup> it was reported that the photocatalytic activity of  $\text{TiO}_2$  nanoparticles can be improved by Sn-doping. In this study, Sn-doped  $\text{TiO}_2$  nanoparticles prepared by the reflux method reported in the literature,<sup>17</sup> were modified by glycidoxypropyltrimethoxysilane (glymo) and they were coated as films having different  $\text{TiO}_2$  contents on glass substrates. A low curing temperature such as 130 °C is suitable for stabilizing the hybrid films. The obtained films had sufficient mechanical integrity, and they were photocatalytically active and could degrade rhodamine B. The main advantage of the employed method is that it is not necessary to calcinate the  $\text{TiO}_2$  particles and a relatively low temperature is sufficient for the curing of the film. This allows the coating of substrates such as plastic, metal, and glass without the application of a barrier layer.

## 2. Results and discussion

### 2.1. Structural and mechanical properties of $\text{TiO}_2$ -glymo films

SEM micrographs of  $\text{TiO}_2$ -glymo films are presented in Figure 1. Sample 1, which has a  $\text{TiO}_2$ -glymo ratio of 0.25, has a crack-free surface without the presence of nanoclusters (Figure 1a). It can be inferred that the high amount of glymo in this film covers all of the  $\text{TiO}_2$  particles and the surface of the glass substrate. With the increase in the  $\text{TiO}_2$  ratio, clusters of about 20 nm form in the films (Figure 1b and 1c). Film thicknesses were measured during SEM examinations (Figure 1d) and the results are presented in Table 1. Film thickness is 5.1  $\mu\text{m}$  when the  $\text{TiO}_2$ -glymo ratio is 0.25. Thickness of the films decreases with the increase in the  $\text{TiO}_2$  content of the film. The film with  $\text{TiO}_2$ -glymo ratio of 7.5 has a thickness of 0.3  $\mu\text{m}$ .

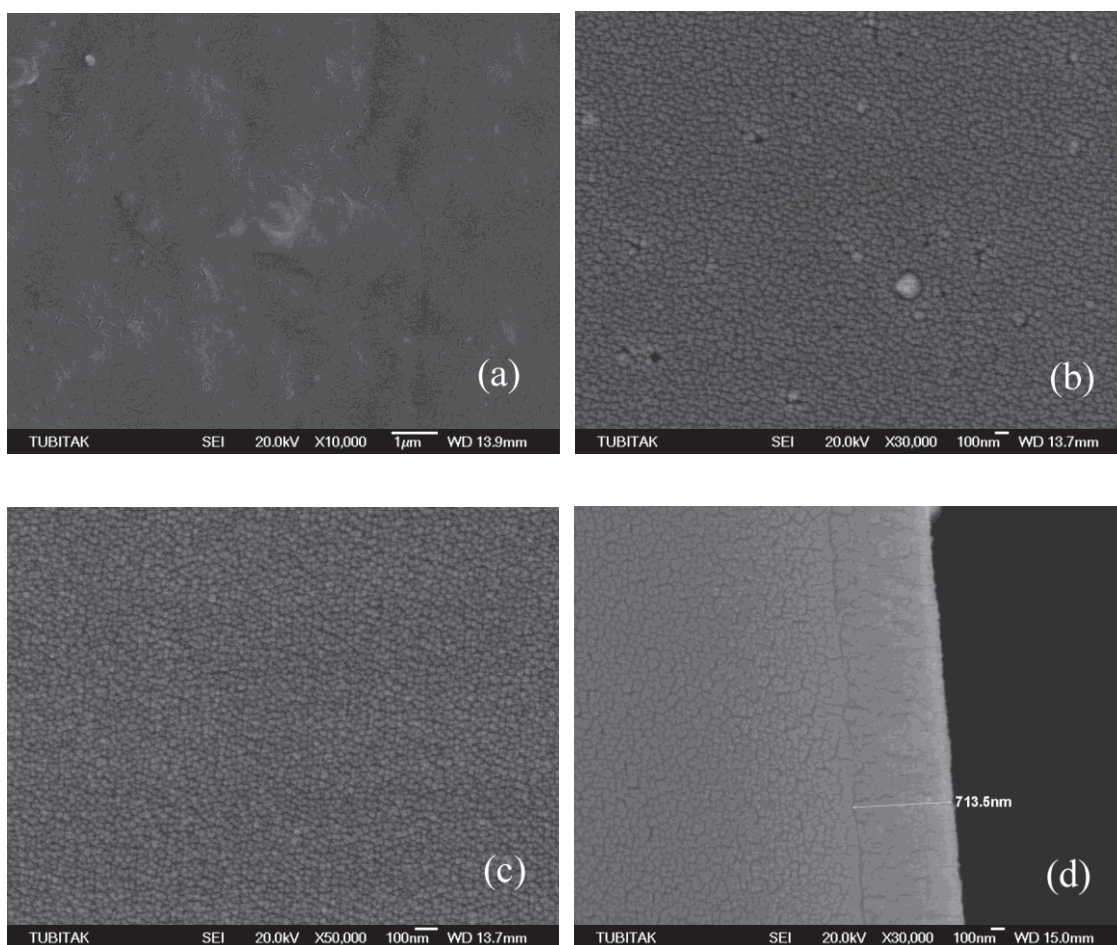


**Figure 1.** SEM micrographs of the top surfaces of (a) sample 1, (b) sample 2, and (c) sample 4 and (d) cross-section of sample 3 (note the difference in magnification).

**Table 1.** Light transmittance, thickness, roughness, pencil hardness, adhesion, and photocatalytic rate constants of TiO<sub>2</sub>-glymo films.

Specimen	TiO <sub>2</sub> /GLYMO (mol)	Film thickness (μm)	Roughness (RMS, m)	Transmittance (%T) at 550 nm (measured by hazemeter)	Haze (%H)	Pencil hardness	Coating adhesion	Rate constant, k (min <sup>-1</sup> )	Half period (min)
1	0.25:1	5.10	108.1	78.9	37.0	2B	5B	0.0032	217
2	0.5:1	1.90	4.8	89.7	0.96	B	5B	0.0038	182
3	2.5:1	0.71	4.3	87.2	0.64	4H	5B	0.0058	120
4	7.5:1	0.30	13.7	84.7	2.28	6H	5B	0.0072	96
Bare glass	-	-		90.5	0.35	-	-	0.0024	289

The coating samples were investigated using AFM, which allows the mapping of global surface roughness compared with SEM. AFM images of TiO<sub>2</sub>-glymo films are presented in Figure 2. The maximum height of the peaks is about 480 nm when the molar ratio of TiO<sub>2</sub> to glymo is 0.25 (Figure 2a). When the ratio is 0.5 or 2.5, the maximum peak height is about 50 (Figures 2b and 2c). This observation was in accord with the results of SEM examinations. Increasing the TiO<sub>2</sub> to glymo ratio to 7.5 resulted in a decrease in the peak

height (Figure 2d); only a few high peaks were present on the films. This may be a result of agglomeration of the  $\text{TiO}_2$  particles when the  $\text{TiO}_2$  to glymo ratio is 7.5. A similar trend was observed in the thicknesses of the films. Thickness of the film decreases with the increase in the  $\text{TiO}_2$  content of the film. RMS roughness values of the films, which are presented in Table 1, are mostly in agreement with the peak heights. RMS roughness decreases from over 100 when the  $\text{TiO}_2$ -glymo ratio is 0.25 to about 4 nm when the ratio is 0.5 or 2.5. It can be inferred that a high amount of glymo in the films increases the roughness. On the other hand, increasing the  $\text{TiO}_2$ :glymo ratio to 7.5 resulted in an increase in the RMS roughness of the films to 13 nm, which may be attributed to the presence of a few high peaks on the film.

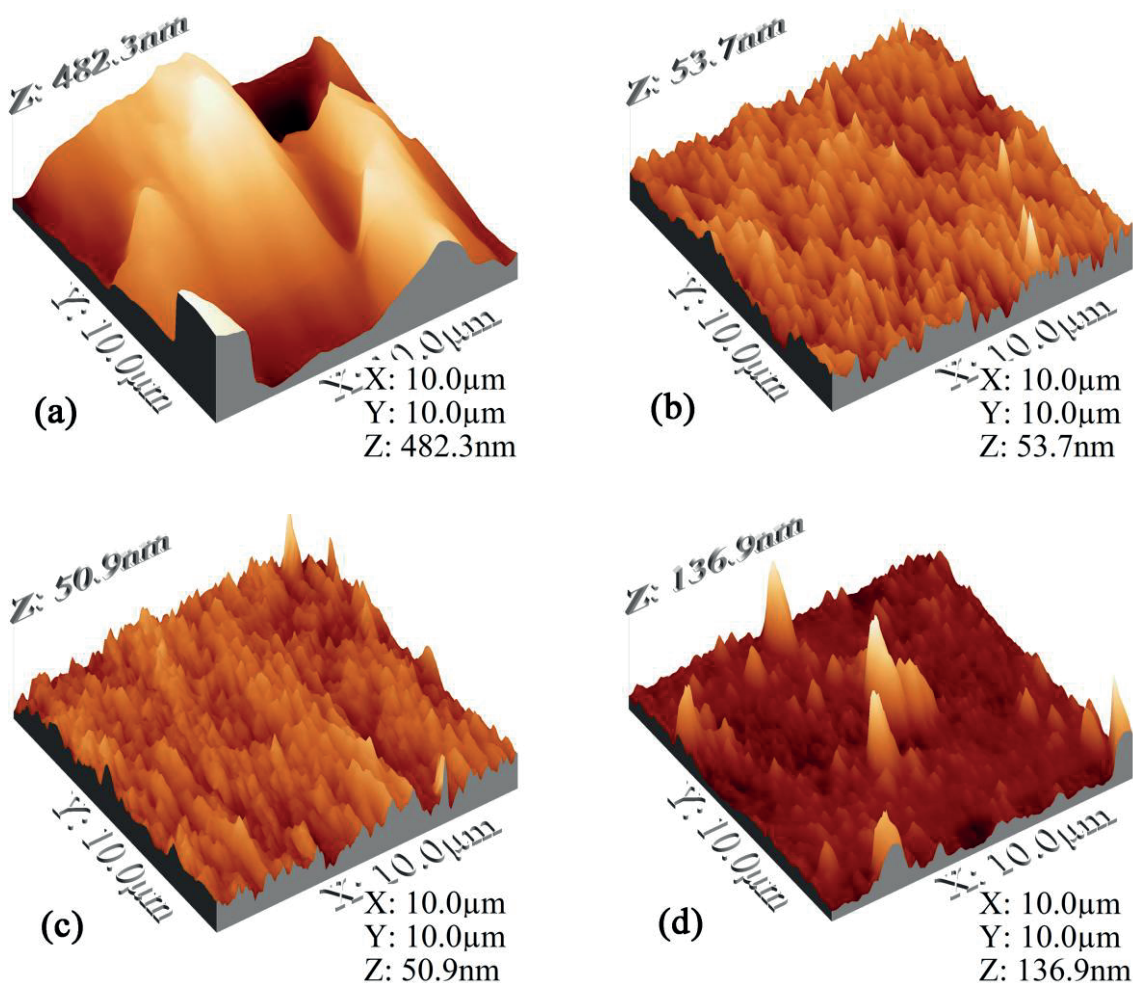


**Figure 2.** AFM images of  $\text{TiO}_2$ -glymo films: (a) sample 1, (b) sample 2, (c) sample 3, (d) sample 4.

Adhesion of the films to the glass surfaces was 5B, indicating that less than 5% of the films was peeled off in the cross-hatch test. On the other hand, pencil hardness of the films was seen to increase with the increase in the  $\text{TiO}_2$  content of the films, as shown in Table 1. This is an expected result since the hardness of  $\text{TiO}_2$  is much higher than that of glymo.

All of the samples having  $\text{TiO}_2$ -glymo films presented lower light transmittance than that of the bare glass, as can be seen in Table 1 and Figure 3. The films cause a decrease in the light transmittance, the extent of which depends on the composition of the film. The film that has the highest glymo ratio presents the lowest

transmittance and it is the haziest among the prepared films. This may be due to the release of methanol in the system during formation of the film, which reduces polarity. Transmittance was seen to first increase with the increase in the  $\text{TiO}_2$  content of the film (when  $\text{TiO}_2$ :glymo is 0.5). Afterwards, a decrease in the transmittance was observed with increasing  $\text{TiO}_2$  content of the film. As the share of  $\text{TiO}_2$  in the films rises, the refractive index of obtained films increases, leading to lower transmittance related to larger reflection of the incident light.

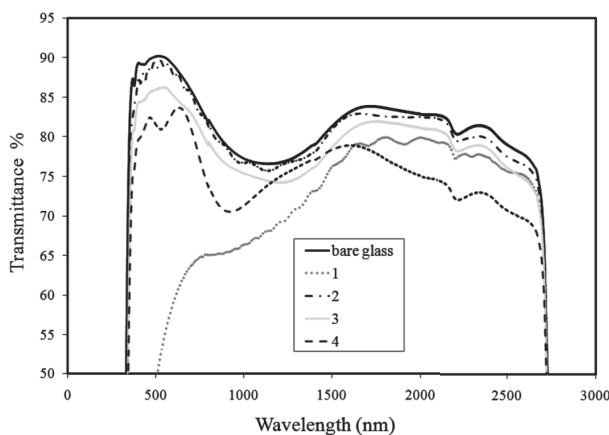


**Figure 3.** Transmittance plots of  $\text{TiO}_2$ -glymo coated glass samples and of bare glass.

In the absence of glymo, crack-free coatings comprising nanoparticles of  $\text{TiO}_2$  are difficult to obtain with thicknesses of more than 100 nm. As the solvent in the coating solution evaporates, the capillary forces between charged nanoparticles drastically increase, promoting the formation of cracks on the surface of  $\text{TiO}_2$  layer. By means of the surface modification of nanoparticles with nonionic substances, e.g., glymo, the influence of capillary effect is reduced or eliminated.  $\text{TiO}_2$  has a high refractive index of 2.56 for anatase. The films of  $\text{TiO}_2$  with thicknesses of less than 100 nm reflect the incident light at a greater rate due to the huge difference in the refractive indices of  $\text{TiO}_2$  film and air. Additionally, the mechanically durable coatings of  $\text{TiO}_2$  nanoparticles are produced by curing at elevated temperatures, at which the application on plastic is not possible. The adhesion of  $\text{TiO}_2$  nanoparticles to plastics is achievable if a layer of primer is applied.

The incorporation of  $\text{TiO}_2$  nanoparticles into a hybrid matrix of glymo lowers the refractive index of the produced film, resulting in less reflectance, i.e. high transparency even at thicknesses of more than 100 nm. The curing of epoxy groups of glymo can be achieved at less than 130 °C, allowing the coating of temperature-sensitive substrates. In this study, glymo served as both a surface modifying agent and a hybrid coating matrix. It allowed the production of nanocompositions on glass with thicknesses up to 5  $\mu\text{m}$  without the formation of cracks. The transparency of studied coatings was varied with the amount of incorporated  $\text{TiO}_2$  nanoparticles. As 5% by weight of  $\text{TiO}_2$  nanoparticles (sample 1) was dispersed in glymo solution, a clear translucent solution was obtained. As solvents were evaporated, however, its coating became slightly turbid and its surface roughness was the highest among the studied samples. This suggests that the larger amount of water in the coating solution compared with the other samples disrupts the stability of  $\text{TiO}_2$  nanoparticles surface-modified with glymo as the organic solvents evaporate faster. The obtained samples 2 and 3 were transparent without visually detectable haze and had low surface roughness. Their transparency was lower than that of bare glass and decreased with an increase in the amount of nanoparticles related to the refractive index of anatase. As for sample 4, the values for both haze and surface roughness rose compared with samples 2 and 3 and the value of its transmittance decreased further. This indicates that the used amount of glymo in sample 4 was barely enough to surface-

modify TiO<sub>2</sub> nanoparticles and form a crack-free, transparent layer. As expected, the increase in the inorganic part of the coatings led to improved surface hardness.

## 2.2. Photocatalytic activity

Photocatalytic activities of the prepared films and uncoated bare glass as a blank can be compared in Figure 4. The photodegradation of rhodamine B occurred in the presence of uncoated glass as a blank under illumination, but its photodegradation considerably increased with the increase in the TiO<sub>2</sub> content of the films. The amount of TiO<sub>2</sub> particles on the surface of the film increased with the TiO<sub>2</sub> content of the films. This may be a significant factor in increasing the activity of the films. The TiO<sub>2</sub> particles that are on the surface of the film and that are in contact with the organic contaminants provide the photocatalytic property to the films. Photocatalytic reaction rate constants of the samples were calculated by plotting  $\ln(C_0/C)$  versus time. In the pseudo first-order rate equation where  $\ln(C_0/C) = kt$ , rate constant  $k$  is evaluated from the slope of the line in  $\ln(C_0/C)$  versus time plot.  $C_0$  is the initial dye concentration,  $C$  is the instantaneous dye concentration,  $k$  is the rate constant ( $\text{min}^{-1}$ ), and  $t$  is time in minutes.<sup>10</sup> Calculated rate constants and the half periods of the samples are presented in Table 1. Sample 4 has the highest rate constant, about  $0.007 \text{ min}^{-1}$ , and sample 3 has a  $k$  value of about  $0.006 \text{ min}^{-1}$ . Half periods of these samples are 96 and 120 min, respectively. Reaction rate constants of the first two samples are much lower than those of the last 2 samples. The effect of TiO<sub>2</sub> concentration in the obtained films on photoactivity can be clearly seen from these results. In our previous studies where TiO<sub>2</sub> films were formed on SiO<sub>2</sub>-coated glass samples, half periods of 300–400 min were obtained. The thickness of the films was in the range of 20–40 nm. It was found that the photoactivity increases with the thickness of the TiO<sub>2</sub> film.<sup>18,19</sup> It can be inferred that photocatalytic activity of TiO<sub>2</sub>-glymo films is higher than that of the TiO<sub>2</sub> films. In the study of Sayilkan et al., TiO<sub>2</sub>-SiO<sub>2</sub> films were prepared by utilizing nanometric TiO<sub>2</sub> particles and tetraethylorthosilicate (TEOS).<sup>10</sup> Photocatalytic activity was reported to increase by increasing the TiO<sub>2</sub> content of the film and by doping TiO<sub>2</sub> with Sn ions. Half periods of the films were 60–120 min,<sup>10</sup> comparable to those calculated in the present study.

## 2.3. Conclusions

Composite coatings consisting of TiO<sub>2</sub> nanoparticles and glymo matrix were prepared by the sol-gel spin-coating method. Molar ratios of TiO<sub>2</sub>:glymo were 0.25, 0.5, 2.5, and 7.5 in the films. Obtained films had sufficient mechanical integrity, and they were photocatalytically active. Film thickness and roughness increased with increasing glymo ratio in the films; however, light transmittance and photoactivity decreased. Sample 3, which has a TiO<sub>2</sub>:glymo ratio of 2.5, may be suggested as the optimum composition. It has a light transmittance of over 85% at 550 nm wavelength, and it has relatively high photocatalytic activity ( $k = 0.0058 \text{ min}^{-1}$ ) and relatively high hardness (4H). It is possible to utilize the composite films on polymer substrates due to the low curing temperature (130 °C). In addition, a barrier layer is not required.

## 3. Experimental

### 3.1. Chemicals and apparatus

The reagents employed were titanium (IV)-*n*-butoxide [Ti(OBu<sup>*n*</sup>)<sub>4</sub> 97%, Fluka] as TiO<sub>2</sub> source, hydrochloric acid (Merck, 37%) as catalyst, tin(IV) chloride (Alfa Aesar, 98%) as dopant, and deionized water as hydrolysis agent. Rhodamine B was used as a model organic pollutant (analytical reagent grade).

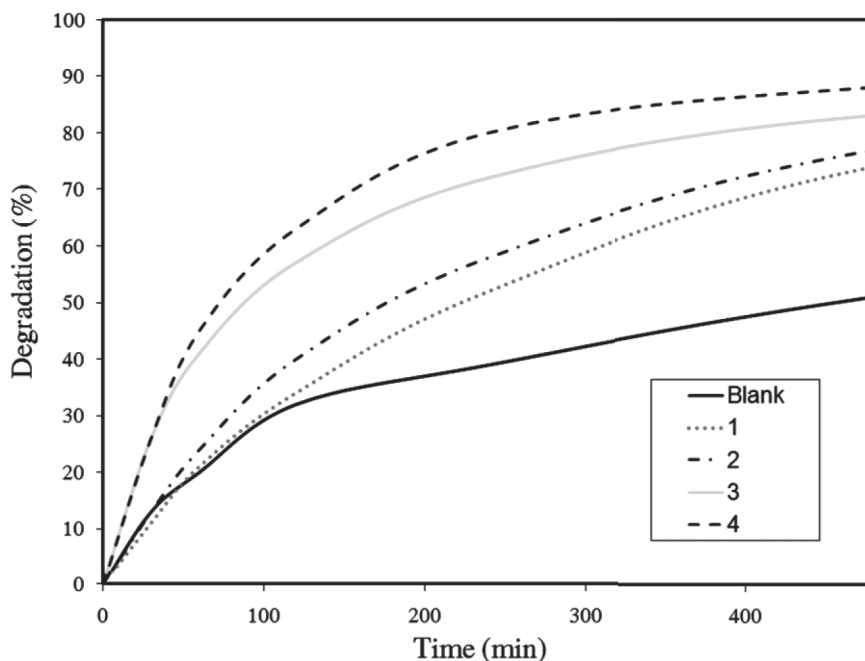


**Figure 4.** Degradation percentages of RhB with time by photocatalytic reaction of coatings having various TiO<sub>2</sub>-glymo ratios and bare glass as blank.

Morphology of the obtained coatings was investigated using scanning electron microscopy (SEM, JEOL JSM 6335-F) and atomic force microscopy (AFM, Quesant Ambios Qscope). The data of AFM micrographs were converted into images by processing with WSxM software.<sup>27</sup>

Surface hardness tests of the films were carried out with an Erichsen Hardness Test Pencil 318. Adhesion tests were performed with an Erichsen Type 295 multicross cutter. The results of the tests were evaluated according to the ASTM D 3359 standard.<sup>28</sup>

In photocatalytic activity tests, a solar box (Erichsen, Model 1500 with a Xenon lamp (1000 W m<sup>-2</sup> in 300–800 nm wavelength range)) was utilized. Dye concentration in the aqueous solution was measured in predetermined durations with a Varian Carry 5000 model UV–Vis–NIR spectrophotometer after irradiation.

### 3.2. Sn-doped TiO<sub>2</sub> powder synthesis

Sn doped-TiO<sub>2</sub> nanopowder was synthesized via the reflux method according to the procedure reported previously,<sup>17,29</sup> in which the synthesized nanoparticles were crystallines of anatase with the size of 5–7 nm. Briefly, Ti(OBu<sup>n</sup>)<sub>4</sub> was hydrolyzed in the presence of hydrochloric acid as a catalyst and tin(IV) chloride as a dopant, then subsequently heat-treated at 130 °C for 5 h. Obtained powders were separated by centrifuging and they were dried in a vacuum oven.

### 3.3. Preparation of TiO<sub>2</sub> sols

TiO<sub>2</sub> sols were prepared by ultrasonically dispersing the synthesized TiO<sub>2</sub> powder (5 g) in a mixture of methoxypropanol (20 g), isopropyl alcohol (20 g), and H<sub>2</sub>O (20 g) (1:1:1 by weight) without using a dispersant. The solvents and the TiO<sub>2</sub> particles were treated in an ultrasonic bath for a few minutes. Finally, transparent TiO<sub>2</sub> sols were obtained.

### 3.4. Preparation of Sn-TiO<sub>2</sub>:glymo films and determination of mechanical properties

Coating solutions were obtained by mixing the dispersed TiO<sub>2</sub> nanoparticles with 3-glycidoxypropyltrimethoxysilane (glymo). In this system, glymo forms the matrix and holds the TiO<sub>2</sub> nanoparticles in the film structure. Glass surfaces were coated with this solution using a spin-coating process. Molar ratios of TiO<sub>2</sub>:glymo were 0.25, 0.5, 2.5, and 7.5 in the films, and amounts of TiO<sub>2</sub> in the sols were kept at 5 wt.%. Ratios of the constituents of the sols and of the films are presented in Table 2. The formation of the composite film can be summarized as in Figure 5. In Figure 5a, 1 mol of glymo is hydrolyzed in the presence of an acid catalyst and 1 mol of H<sub>2</sub>O. After that, it can be seen in Figure 5b that the epoxy group in the glymo opens due to titanium, which is a Lewis acid. The proposed mechanism for epoxy ring opening of glymo was reported in the literature.<sup>30,31</sup> The bonding between the groups that are present on the surface of the TiO<sub>2</sub> particles and the matrix can be seen in Figure 5c. Finally, surfaces of the TiO<sub>2</sub> nanoparticles are modified with the prehydrolyzed glymo by the aid of water and alcohol condensation.

**Table 2.** Ratios of the constituents of the sols and films.

Specimen	TiO <sub>2</sub> (mol)	GLYMO (mol)	TiO <sub>2</sub> /GLYMO (mol)	TiO <sub>2</sub> (g)	Glymo (g)	IPA:PM (1:1) (w:w)	H <sub>2</sub> O(g)	TiO <sub>2</sub> % w/w (in sol)	TiO <sub>2</sub> % w/w (in coating)
1	0.0127	0.051	0.25:1	1.0145	12.036	4.459	2.754	5	10
2	0.0086	0.0172	0.5:1	0.687	4.0592	8.065	0.929	5	26
3	0.0135	0.0054	2.5:1	1.0784	1.2744	18.924	0.292	5	53
4	0.0135	0.0018	7.5:1	1.0784	0.4248	19.968	0.097	5	77

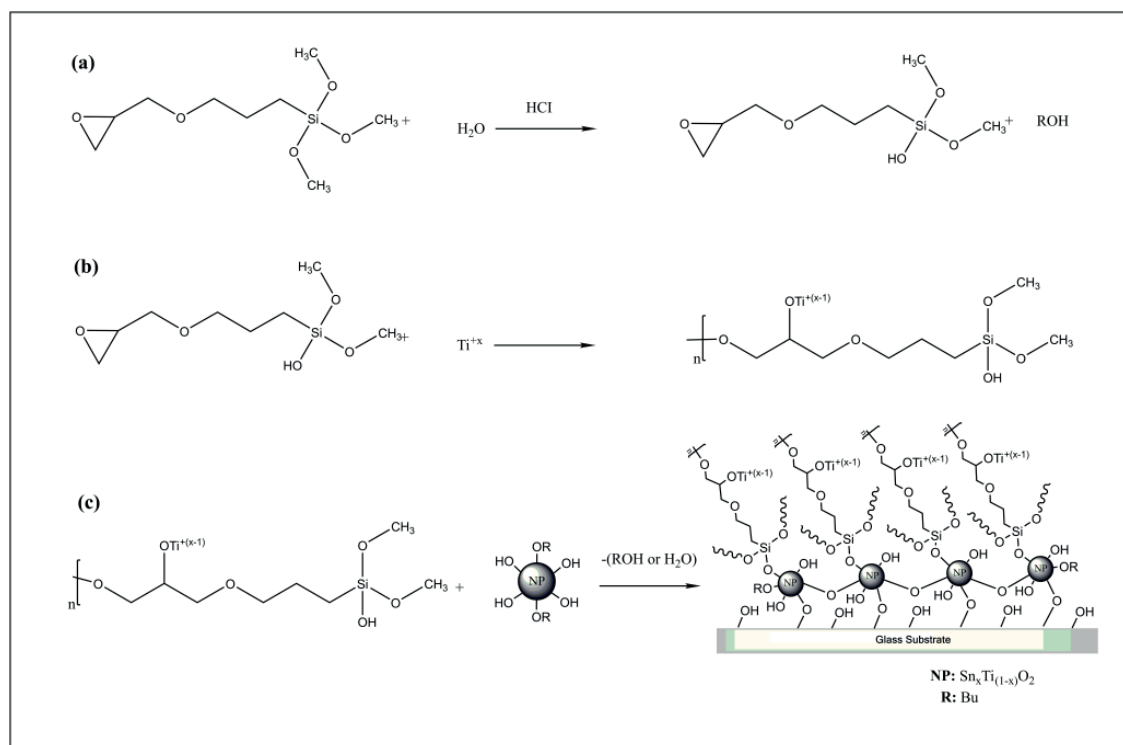


**Figure 5.** (a) Hydrolysis of glymo, (b) epoxy ring opening mechanism by titanium ions, (c) surface modification of TiO<sub>2</sub> with glymo and the formation of film on glass substrate.



### 3.5. Photocatalytic degradation of rhodamine B

In order to determine the photocatalytic activity, rhodamine B (RhB) degradation tests were performed. Samples having 2.5 cm × 2.5 cm dimensions were cut out from the coated 10 cm × 10 cm substrates. Transparent cylindrical polystyrene boxes with 3 cm diameter and 6 cm height were filled with 15 mL of RhB and deionized water solution, which had a concentration of 1 mg L<sup>-1</sup>. Two parallel sets of coated glass samples and uncoated glass substrates as a blank were placed into the boxes containing RhB solutions and the boxes were kept inside the solar box. The samples in the solar box were kept 20 cm away from the lamp, which simulates the spectrum of the sunlight including the UV and visible parts of it. The variation of the RhB concentration was monitored by analyzing the absorbance of solutions by UV-Vis-NIR spectrophotometer in predetermined intervals for a total duration of 8 h.

### Acknowledgment

The authors thank the Akdeniz University Research Fund for financial support.

### References

1. Ahmed, S.; Rasul, M. G.; Martens, W.; Brown, R.; Hashib, M. A. *Water Air Soil Pollut.* **2011**, *215*, 3-29.
2. Dey, N. K.; Kim, M. J.; Kim, K. D.; Seo, H. O.; Kim, D.; Kim, Y. D.; Lim, D. C.; Lee, K. H. *J. Mol. Catal. A Chem.* **2011**, *337*, 33-38.
3. Segota, S.; Curkovic, L.; Ljubas, D.; Svetlicic, V.; Houra, I. F.; Tomasic, N. *Ceram. Int.* **2011**, *37*, 1153-1160.
4. Bellardita, M.; Addamo, M.; Di Paola, A.; Palmisano, L. *Chem. Phys.* **2007**, *339*, 94-103.
5. Shi, J. W.; Zheng, J. T.; Wu, P. *J. Hazard. Mater.* **2009**, *161*, 416-422.
6. Chen, Q.; Jiang, D.; Shi, W.; Wu, D.; Xu, Y. *Appl. Surf. Sci.* **2009**, *255*, 7918-7924.
7. Fan, C.; Xue, P.; Sun, Y. *J. Rare Earth* **2006**, *24*, 309-313.
8. Lu, X.; Ma, Y.; Tian, B. Zhang J. *Solid State Sci.* **2011**, *13*, 625-629.
9. Pärna, R.; Joost, U.; Nõmmiste, E.; Käämbre, T.; Kikas, A.; Kuusik, I.; Hirsimäki, M.; Kink, I.; Kisand, V. *Appl. Surf. Sci.* **2011**, *257*, 6897-6907.
10. Sayilkan, F.; Asilturk, M.; Tatar, P.; Kiraz, N.; Sener, S.; Arpac, E.; Sayilkan, H. *Mater. Res. Bull.* **2008**, *43*, 127-134.
11. Sayilkan, F.; Asilturk, M.; Tatar, P.; Kiraz, N.; Arpac, E.; Sayilkan, H. *J. Hazard. Mater.* **2007**, *144*, 140-146.
12. Tong, T.; Zhang, J.; Tian, B.; Chen, F.; He, D. *J. Hazard. Mater.* **2008**, *155*, 572-579.
13. Xu, A. W.; Gao, Y.; Liu, H. Q. *J. Catal.* **2002**, *207*, 151-157.
14. Yao, M. S.; Chen, J. H.; Zhao, C. H.; Chen, Y. *Thin Solid Films* **2009**, *517*, 5994-5999.
15. Štengl, V.; Bakardjieva, S.; Murafa, N. *Mater. Chem. Phys.* **2009**, *114*, 217-226.
16. Wang, Z.; Chen, C.; Wu, F.; Zou, B.; Zhao, M.; Wang, J.; Feng, C. *J. Hazard. Mater.* **2009**, *164*, 615-620.
17. Kiraz, N.; Burunkaya, E.; Kesmez, O.; Camurlu, H. E.; Asilturk, M.; Yesil, Z.; Arpac, E. *J. Sol-Gel Sci. Technol.* **2011**, *59*, 381-386.
18. Burunkaya, E.; Kesmez, O.; Kiraz, N.; Camurlu, H. E.; Asilturk, M.; Arpac, E. *Mater. Chem. Phys.* **2010**, *120*, 272-276.
19. Kesmez, O.; Camurlu, H. E.; Burunkaya, E.; Arpac, E. *Sol. Energy Mater. Sol. Cells* **2009**, *93*, 1833-1839.
20. Della Foglia, F.; Losco, T.; Piseri, P.; Milani, P.; Selli, E. *J. Nanopart. Res.* **2009**, *11*, 1339-1348.

21. Horprathum, M.; Eiamchai, P.; Limnonthakul, P.; Nuntawong, N.; Chindaudom, P.; Pokaipisit, A.; Limsuwan, P. *J. Alloys Compd.* **2011**, *509*, 4520-4524.
22. Vernardou, D.; Stratakis, E.; Kenanakis, G.; Yates, H. M.; Couris, S.; Pemble, M. E.; Koudoumas, E.; Katsarakis, N. *J. Photochem. Photobiol. A Chem.* **2009**, *202*, 81-85.
23. Elfanaoui, A.; Elhamri, E.; Boukaddat, L.; Ihlal, A.; Bouabid, K.; Laanab, L.; Taleb, A.; Portier, X. *Int. J. Hydrogen Energy* **2011**, *36*, 4130-4133.
24. Gohin, M.; Allain, E.; Chemin, N.; Maurin, I.; Gacoin, T.; Boilot, J. P. *J. Photochem. Photobiol. A Chem.* **2010**, *216*, 142-148.
25. Zita, J.; Krysa, J.; Cernigoj, U.; Lavrencic-Stangar, U.; Jirkovsky, J.; Rathousky, J. *Catal. Today* **2011**, *161*, 29-34.
26. Zita, J.; Maixner, J.; Krysa, J. *J. Photochem. Photobiol. A Chem.* **2010**, *216*, 194-200.
27. Horcas, I.; Fernandez, R.; Gomez-Rodriguez, J. M.; Colchero, J.; Gomez-Herrero, J.; Baro, A. M. *Rev. Sci. Instrum.* **2007**, *78*, 013705.
28. Schmidt, H. *J. Non-Cryst. Solids* **1994**, *178*, 302-312.
29. Burunkaya, E.; Yeşil, Z.; Kesmez, Ö.; Kiraz, N.; Çamurlu, H. E.; Arpaç, E. In *NanoTR VII 2011 - Nanoscience and Nanotechnology Conference*; June 2011, İstanbul, Turkey.
30. Kayan, A. *J. Appl. Polym. Sci.* **2012**, *123*, 3527-3534.
31. Hoebbel, D.; Nacken, M.; Schmidt, H. *J. Sol-Gel Sci. Technol.* **2001**, *21*, 177-187.